

AperTO - Archivio Istituzionale Open Access dell'Università di Torino

Phototransformation study of the antidepressant paroxetine in surface waters

This is a pre print version of the following article:

Original Citation:

Availability:

This version is available <http://hdl.handle.net/2318/1838098> since 2022-02-03T09:01:51Z

Published version:

DOI:10.1016/j.scitotenv.2021.145380

Terms of use:

Open Access

Anyone can freely access the full text of works made available as "Open Access". Works made available under a Creative Commons license can be used according to the terms and conditions of said license. Use of all other works requires consent of the right holder (author or publisher) if not exempted from copyright protection by the applicable law.

(Article begins on next page)

Phototransformation study of the antidepressant paroxetine in surface waters

Tjasa Gornik^{a,b,1}, Luca Carena^{c,1}, Tina Kosjek^{a,b,*}, Davide Vione^{c,**}

^a *Jozef Stefan Institute, Department of Environmental Sciences, Jamova 39, Ljubljana, Slovenia*

^b *Jozef Stefan International Postgraduate School, Jamova 39, Ljubljana, Slovenia*

^c *Department of Chemistry, University of Torino, Via Pietro Giuria 5, 10125 Torino, Italy.*

*Corresponding author: Jozef Stefan Institute, Jamova 39, 1000, Ljubljana, Slovenia. Tel.: +38614773288.

**Corresponding author: Department of Chemistry, University of Torino, Via Pietro Giuria 5, 10125 Torino, Italy.

¹Joint first authors.

E-mail addresses: tina.kosjek@ijs.si (T. Kosjek), davide.vione@unito.it (D. Vione)

ABSTRACT

In this work, the photochemistry of the antidepressant paroxetine and its photochemical fate in surface waters were investigated. The direct photolysis quantum yield, as well as the second-order rate constants of the reactions between paroxetine and the photochemically produced reactive intermediates (i.e., HO[•], ³CDOM* and ¹O₂) were assessed with steady-state irradiation experiments. Using these results, the paroxetine photochemical fate (i.e., pseudo-first order photodegradation rate constant and half-life time) was modeled in a surface-water scenario by varying the chemical composition of water and its depth. Nine transformation products were identified, formed upon paroxetine direct and indirect photolysis, and a photodegradation

pathway was proposed that is initiated by photohydrolysis of paroxetine to 4-(4-fluorophenyl)-3-(hydroxymethyl)piperidine. Finally, the occurrence of paroxetine and its transformation products was investigated in Slovenian surface waters, also predicting the compound's lifetime in Slovenian water bodies based on the 2018 chemical composition data.

The results showed that paroxetine reacts with HO[•] radicals approaching a diffusion-controlled kinetics, while the direct photolysis quantum yield is $\Phi_{\text{PXT}} = (4.03 \pm 0.25) \times 10^{-2}$. Direct photolysis, together with reactions with HO[•] and CO₃^{•-} radicals would be the main photodegradation pathways for paroxetine in surface waters. Reaction with CO₃^{•-} is particularly important for low amounts of dissolved organic matter (DOM).

KEYWORDS

Direct photolysis; Hydroxyl radical; Transformation product; Photochemical modelling; Piperidine, Photodegradation.

1. Introduction

Paroxetine (hereafter PXT) is an antidepressant of the selective serotonin reuptake inhibitors (SSRI) class. It is the 57th on the list of the Top 200 prescribed drugs in the US (Fuentes et al., 2018), and the 17th on the list of most prescribed psychiatric drugs in the US (McDermott, 2018). Its main source in the environment is human excretion. In the human body, PXT undergoes extensive phase I and II metabolism, including oxidation to its catechol (PC), followed by formation of the methyl intermediate (PM), and by conjugation (glucuronidation, sulfation) (Matsunaga et al., 2013). Therefore, less than 1% of the ingested PXT is excreted as the parent compound.

Cunningham et al. (2004) discussed the hydrolysis of conjugates back to the parent compound or PM in wastewater (WW) treatment systems, suggesting that PXT and PM are the main candidates for monitoring after they enter the aqueous environment. The group then studied the PXT and PM behavior in activated sludge (AS) biodegradation experiments, where PM was extensively removed by both sorption and biodegradation. They also reported that PXT was only removed by sorption to AS. Nevertheless, Radjenović et al. (2007) showed high removal of PXT in both, the conventional AS process (90.6%) and in membrane bioreactors (89.7%) irrespective of the removal mechanism. Despite this, PXT has repeatedly been detected in different environmental compartments (*e.g.*, WW, surface waters (SW), sediment, fish tissue) (Arnnok et al., 2017; Mole and Brooks, 2019; Schultz et al., 2010; Vasskog et al., 2008, 2006). The reported concentration in SW is generally a few ng L⁻¹. The highest concentrations up to date were reported in the western Lake Erie basin (90 ng L⁻¹) and the Niagara river (270 ng L⁻¹) (Arnnok et al., 2017; Wu et al., 2009). Until now, no data exist on the occurrence of PXT metabolites or transformation products (TPs) in environmental matrices.

Once in the environment, PXT causes neurohormone-like adverse effects in aquatic organisms (e.g. changes in reproduction), similarly as other antidepressants from the SSRI class. Its acute toxicity has been studied on model aquatic organisms of lower trophic levels, where the effects are expected to be the most pronounced (e.g., *C. dubia*, *D. magna*, *D. polymorpha*, *S. striatum*, *P. elliptica*, *H. tuberculata*, *X. laevis*) (Fong, 2001; Silva et al., 2015). In comparison, the acute toxicity of PM for aquatic organisms has also been estimated based on tests on *D. magna*, indicating a low risk of any adverse effects arising from the exposure to PM (Cunningham et al., 2004). Hence, the reason for choosing PXT as our focus compound lies in the processes occurring during WW treatment and the results of toxicity tests.

The available literature on the breakdown of PXT after it has reached the environment is quite limited. However, authors agree on photodegradation being one of the main processes of PXT elimination (Cunningham et al., 2004; Henry et al., 2004; Kwon and Armbrust, 2004; Santoke and Cooper, 2017; US Environmental Protection Agency, 2016). In general, photodegradation of a water pollutant can occur through two main pathways, namely direct and indirect photolysis. Direct phototransformation takes place when the compound absorbs solar radiation and gets transformed because of the obtained extra-energy. In contrast, indirect photochemistry involves the reactions between the xenobiotic and the *Photochemically Produced Reactive Intermediates* (PPRIs), which are formed upon sunlight absorption by natural photosensitizers such as the chromophoric dissolved organic matter (CDOM), nitrate and nitrite (Vione et al., 2014). The main PPRIs in SW are hydroxyl and carbonate radicals (HO^\bullet and $\text{CO}_3^{\bullet-}$, respectively), the excited triplet states of CDOM ($^3\text{CDOM}^*$) and singlet oxygen ($^1\text{O}_2$). Kwon and Armbrust (2004) have previously performed irradiation experiments in both synthetic buffer-solutions and lake water with a fluorescent light. Santoke and Cooper (2017) have found that HO^\bullet and $^1\text{O}_2$ play a role in

PXT photodegradation in irradiated Suwannee river water samples. Reportedly, photodegradation occurs fast and in a large percentage (Kwon and Armbrust, 2004; Santoke and Cooper, 2017), which implies that TPs could be responsible for the majority of toxic effects and might be better suited as markers of PXT environmental presence (Cunningham et al., 2004; Kwon and Armbrust, 2004). Nonetheless, it is clear from the available literature that there is still a lack of information concerning the relative importance of direct and indirect photochemistry on the environmental fate of PXT, including the formation of other TPs and the relevance of different transformation pathways. The roles of direct photolysis and the reactions with $^3\text{CDOM}^*$ and $\text{CO}_3^{\bullet-}$, which are known to be important transformation pathways for xenobiotics (Canonica, 2007; Wojnárovits et al., 2020), have still to be determined in the case of PXT.

To fill in this knowledge gap our research involved: (a) laboratory-scale irradiation experiments to determine the PXT photoreactivity parameters (i.e., direct photolysis quantum yield and the second-order reaction rate constants between PXT and the main PPRIs); (b) modeling of PXT photochemical fate in surface water; (c) identification of the TPs formed upon PXT direct and indirect phototransformation, by means of high resolution/accurate mass-mass spectrometry (HR/AM MS); (d) determination of PXT TPs in actual SW samples.

2. Materials and methods

2.1 Standards, chemicals and materials

The data on the standards, chemicals and materials we used can be found in the Supplementary material (SM), **Chapter 1.1**. The preparation procedure of stock solutions is reported in SM, **Chapter 1.2**.

2.2 Irradiation Experiments

Irradiation runs were performed with different lamps, depending on the aim of the experiment:

- 1) A Philips narrow band TL 20W/01 lamp, which mainly emits in the UVB range of the light spectrum (emission maximum at 313 nm).
- 2) A UVA black lamp (Philips TL-D 18 W), with emission maximum at 369 nm.
- 3) A Philips TL D 18W/16 Yellow lamp, the emission spectrum of which is reported elsewhere (Carena et al., 2017; Rosario-Ortiz and Canonica, 2016; Vione, 2020).

Chemical actinometry with 2-nitrobenzaldehyde (Carena et al., 2019; Galbavy et al., 2010; Willett and Hites, 2000) was used to determine the spectral photon flux density occurring in the irradiated solutions.

In general, aqueous solutions (5 or 20 mL) containing *(i)* PXT, *(ii)* a suitable photosensitizer (which selectively produces a given PPRI) and (when relevant) *(iii)* a PPRI scavenger, were put in Pyrex glass cells and magnetically stirred under steady irradiation. The solution pH ranged between 6 and 7. After scheduled irradiation times, solutions were withdrawn and analyzed for PXT with a high-performance liquid chromatograph, equipped with a diode-array detector (HPLC-DAD, Hitachi LaChrom Elite® series).

The time trends of the PXT concentration followed pseudo-first order kinetics, namely $[PXT] = [PXT]_0 \times e^{-k' \times t}$, where $[PXT]_0$ is the initial concentration of paroxetine (*vide infra* for its values), k' the pseudo-first order rate constant of PXT degradation, and t the irradiation time. After assessing k' from the data fit of $[PXT]$ vs. t , the initial PXT degradation rate was calculated as $R = k' \times [PXT]_0$.

Irradiation experiments aimed at identifying the paroxetine TPs were carried out in aqueous solutions (20 mL) containing PXT (100 $\mu\text{mol L}^{-1}$) and a selective photosensitizer. In particular, hydrogen peroxide (5 mmol L^{-1}) and NaNO_3 (10 mmol L^{-1}) were separately used for HO^\bullet -induced reactions, benzophenone-4-carboxylate (CBBP, 70 $\mu\text{mol L}^{-1}$) for transformation by $^3\text{CDOM}^*$, and Rose Bengal (RB, 10 $\mu\text{mol L}^{-1}$) for transformation by $^1\text{O}_2$. Finally, a mixture of NaNO_3 (10 mmol L^{-1}) and NaHCO_3 (0.8 mol L^{-1}) was used as photosensitizer to produce $\text{CO}_3^{\bullet-}$ radicals. After collection, samples were analyzed for TP identification by means of ultra-high-performance liquid chromatography coupled to a hybrid quadrupole time-of-flight mass spectrometry (UHPLC-QToF, Waters Quattro Premier series).

2.3 Sample preparation and instrumental analysis

Samples obtained from the irradiation experiments (**section 2.2**) were injected into HPLC-DAD or UHPLC-QToF without additional preparation.

The determination of PXT concentration in SW samples (**section 2.5**) was carried out using a ultra-high performance liquid chromatograph UHPLC (Shimadzu Nexera X2) - hybrid quadrupole-linear ion trap mass spectrometry analyzer (Sciex Qtrap 4500). Before injection, samples were pre-concentrated and cleaned by solid phase extraction (SPE) on Strata XC cartridges. The 250-mL aliquots of each sample were first spiked with PXT-D₆ as an internal

standard at the final concentration of 30 ng L^{-1} , and then filtered through Whatman GF/C filters. The pH value was adjusted to 2 with 37% HCl and the samples were loaded onto cartridges preconditioned with 3 mL of MeOH, and equilibrated with 3 mL of HCl-acidified ultrapure water (pH 2) at a flow rate of $6\text{-}7 \text{ mL min}^{-1}$. Matrix interferences were washed off with 10% methanol (MeOH) in ultrapure water. PXT was eluted with $3 \times 0.6 \text{ mL}$ of 5% NH_4OH in MeOH. The extracts were dried at $30 \text{ }^\circ\text{C}$ under nitrogen flow, and then reconstituted in $100 \text{ }\mu\text{L}$ of 20% MeOH in 0.1% formic acid. Samples were prepared in duplicates. The occurrence of TPs was checked in the same extracts.

The exact operating conditions for each instrumental analysis can be found in SM, **Chapter 1.3**.

Information on the analytical method validation is reported in SM, **Chapter 1.4**.

2.4 Identification of TPs formed by PXT photodegradation

The identification was performed with UHPLC-QToF. The screening approaches were accomplished in the targeted way, where the TPs reported in the literature and candidates predicted from potential phototransformation reactions were manually screened for ("suspect list") (Kwon and Armbrust, 2004; Matsunaga et al., 2013; Vay et al., 2018; Zhao et al., 2007). In addition, we screened for potential TPs using the non-targeted approach with the open-source package MZmine (version 2.53). The analysis of data obtained with liquid chromatography coupled to mass spectrometry (LC-MS) was performed similarly as in Gornik et al. (2020). Data were transformed from raw files into mzML format using Proteowizard (version 3.0.20075) software, before being processed in MZmine. The peaks were detected by first using the centroid mass algorithm, followed by chromatogram building. For the deconvolution of the obtained chromatograms, wavelet (Automated Data Analysis Pipeline (ADAP)) algorithm was utilized

(Myers et al., 2017). Deisotoping was done by applying the isotopic peaks grouper algorithm with the RT tolerance of 0.2 min, a m/z tolerance of 25 ppm, and the lowest m/z value as the representative isotope. The peak list alignment algorithm Random Sample Consensus (RANSAC) was applied to the list and gap filling was performed based on the m/z tolerance of 25 ppm. The list of features was filtered and the obtained list of candidates was further evaluated to exclude the compounds present in blanks or control samples. The remaining candidates were tentatively identified based on their MS/MS spectra using Mass Lynx v 4.1. The criteria for TP identification included: 1) a maximum error of 15 ppm between the measured and theoretical mass of the protonated parent molecule, and 40 ppm for its product ions; 2) isotopic pattern score over 80% where available; 3) reasonable ring double bond equivalents (RDBE) value. The chemical structures and transformations were drawn in ChemDraw Ultra 12.0.2 (Perkin Elmer).

2.5 Occurrence of PXT and its TPs in Slovenian SW

We collected six-hour composite samples of three Slovenian rivers (A, B and C) in order to investigate the occurrence of PXT and its TPs. The exact sampling locations and dates can be found in **Table S-4** (SM). The values of pH and dissolved oxygen (DO) of the river water at each sampling point were measured with a multi-parameter portable meter MultiLine® Multi 3630 IDS (WTW, Weilheim, Germany).

3. Results and discussion

3.1 Irradiation experiments

3.1.1 PXT direct photolysis

The direct photolysis of PXT was assessed under UVB irradiation (see **Fig.1a** for the lamp spectrum, *i.e.*, the spectral photon flux density in the irradiated solutions). Although sunlight has relatively low irradiance in the UVB region, UVB radiation should account for the vast majority of PXT direct photolysis in the environment. Indeed, PXT efficiently absorbs sunlight at $\lambda < 320$ nm (**Fig.1a**), while negligible radiation absorption occurs in the UVA and visible regions. This issue, together with the fact that the direct photolysis quantum yields are measured more accurately under narrow-band radiation, justified the choice of the UVB lamp.

PXT ($20 \mu\text{mol L}^{-1}$) was irradiated in ultrapure water (5 mL) under UVB light for up to 150 min (**Fig.1b**). In such conditions, the rate of PXT direct photolysis is expressed as

$R_{d.p.} = \Phi_{PXT} \times \int_{\lambda_1}^{\lambda_2} p^0(\lambda) \times [1 - 10^{-\varepsilon_{PXT}(\lambda) \times b \times [PXT]}] d\lambda$, where $p^0(\lambda)$ is the lamp spectral photon flux density (**Fig.1a**), $\varepsilon_{PXT}(\lambda)$ is the molar absorption coefficient of PXT (**Fig.1a**), b is

the light optical path in solution (0.4 cm), and Φ_{PXT} is the apparent quantum yield of PXT direct

photolysis. It was $R_{d.p.} = 2.41 \pm 0.10 \text{ nmol L}^{-1} \text{ s}^{-1}$, and the photon flux absorbed by PXT was P_a

$= \int_{\lambda_1}^{\lambda_2} p^0(\lambda) \times [1 - 10^{-\varepsilon_{PXT}(\lambda) \times b \times [PXT]}] d\lambda = (5.97 \pm 0.36) \times 10^{-8} \text{ Einstein L}^{-1} \text{ s}^{-1}$. As a

consequence, one gets $\Phi_{PXT} = R_{d.p.} (P_a)^{-1} = (4.03 \pm 0.25) \times 10^{-2}$.

The obtained value of Φ_{PXT} is ~ 5 times lower than that measured at $\lambda = 254$ nm in previous work, although with high uncertainty ($\Phi_{PXT}(254 \text{ nm}) = 0.21 \pm 0.14$; (Wols et al., 2014)). Such a

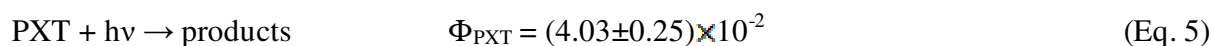
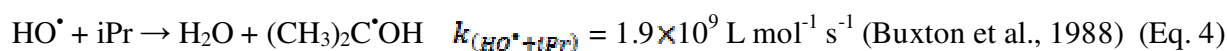
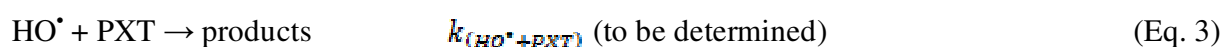
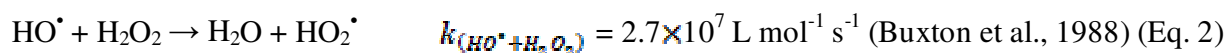
difference in the photolysis quantum yield values measured for a certain pharmaceutical (Challis et al., 2014) could be accounted for by the use of dissimilar irradiation wavelengths. Indeed, although the phototransformation quantum yields of polyatomic organic molecules often follow Kasha's rule (Turro et al., 1978), it is not uncommon to find a wavelength dependence in the quantum yields of photochemical reactions (Demchenko et al., 2017). In the case of PXT, the UVB quantum yield would be representative of phototransformation under sunlight, differently from the 254-nm quantum yield.

3.1.2 Reaction with HO[•] radicals

The second-order rate constant of the reaction between PXT and HO[•] radical ($k_{(HO^{\bullet}+PXT)}$) was assessed by exploiting the competition between PXT and isopropanol (2-propanol, hereinafter iPr) for reaction with HO[•] (Carena et al., 2018). iPr is a well-known HO[•] scavenger, which reacts with HO[•] radicals mainly through hydrogen abstraction, with a rate constant $k_{(HO^{\bullet}+iPr)} = 1.9 \times 10^9$ L mol⁻¹ s⁻¹ (Buxton et al., 1988).

Aqueous solutions (5 mL) containing H₂O₂ (5 mmol L⁻¹), PXT (20.2 μmol L⁻¹) and iPr (from 0 to 3 mmol L⁻¹) were irradiated under UVB light, in which conditions H₂O₂ is an efficient HO[•] photosensitizer. The potential reactions taking place during irradiation of these solutions are the formation of HO[•] radicals upon H₂O₂ photolysis (**Eq.1**), the concurrent scavenging of HO[•] by H₂O₂, PXT and iPr (**Eqs.2,3,4**), as well as the direct photolysis of PXT (**Eq.5**). Actually, these reactions are not the only ones that occur in the system, but they are the most important in the assessment of $k_{(HO^{\bullet}+iPr)}$. Additionally, the reaction between HO[•] and iPr mainly forms the α-hydroxyalkyl radical (CH₃)₂C[•]OH, which can react with dissolved O₂ to produce superoxide radical, H₂O₂, acetone and other small organic compounds (von Sonntag and Schuchmann,

1991). Because the degradation of iPr by HO[•] produces several radical species (here generally defined as X[•]), the possible reactions between PXT and X[•] (Eq.6) should not be ruled out *a priori*.



The overall degradation rate of PXT (R_{tot}) can be described as the sum $R_{\text{tot}} = R_{(\text{PXT} + \text{HO}^\bullet)} + R_{\text{d.p.}} + R_{\text{add}}$, where $R_{(\text{PXT} + \text{HO}^\bullet)}$, $R_{\text{d.p.}}$, and R_{add} are the rates of Eqs. 3, 5 and 6, respectively. $R_{\text{d.p.}}$ was measured as $2.7 \pm 0.3 \text{ nmol L}^{-1} \text{ s}^{-1}$ (Fig.2a), in good agreement with the value of $2.4 \pm 0.1 \text{ nmol L}^{-1} \text{ s}^{-1}$ reported in the previous section. This is due to the fact that UVB radiation absorption by H₂O₂ is low enough, not to interfere significantly with the direct photolysis of PXT.

R_{tot} was measured at different iPr concentrations, and then corrected for $R_{\text{d.p.}}$ (i.e., $R_{\text{tot}} - R_{\text{d.p.}} = R_{(\text{PXT} + \text{HO}^\bullet)} + R_{\text{add}}$). The sum $R_{(\text{PXT} + \text{HO}^\bullet)} + R_{\text{add}}$ decreased with increasing alcohol concentration (Fig.2b), because of the competition between iPr and PXT for reaction with HO[•]. Competition kinetics can be modeled by considering that $R_{(\text{PXT} + \text{HO}^\bullet)} = k_{(\text{HO}^\bullet + \text{PXT})} \times [\text{HO}^\bullet] \times [\text{PXT}]$, and by reasonably adopting the steady-state

approximation for the hydroxyl radicals concentration ($[HO^\bullet]$). By taking into account the formation of HO^\bullet and its consumption by H_2O_2 , PXT and iPr, one gets $R_{f,HO^\bullet} = [HO^\bullet] \times (k_{(HO^\bullet+H_2O_2)} \times [H_2O_2] + k_{(HO^\bullet+PXT)} \times [PXT] + k_{(HO^\bullet+iPr)} \times [iPr])$, where R_{f,HO^\bullet} is the formation rate of HO^\bullet radicals upon H_2O_2 photolysis (Eq.1). By replacing the value of $[HO^\bullet]$ thus obtained in the expression for $R_{(PXT+HO^\bullet)}$, one gets the following:

$$R_{(PXT+HO^\bullet)} + R_{add} = \frac{R_{f,HO^\bullet} \times k_{(HO^\bullet+PXT)} \times [PXT]}{k_{(HO^\bullet+H_2O_2)} \times [H_2O_2] + k_{(HO^\bullet+PXT)} \times [PXT] + k_{(HO^\bullet+iPr)} \times [iPr]} + R_{add} \quad (\text{Eq. 7})$$

Eq.7 was used to fit the experimental data reported in Fig.2b, with R_{f,HO^\bullet} , $k_{(HO^\bullet+PXT)}$ and R_{add} as fit variables, yielding $k_{(HO^\bullet+PXT)} = (1.7 \pm 0.5) \times 10^{10} \text{ L mol}^{-1} \text{ s}^{-1}$. Although slightly higher, this value of $k_{(HO^\bullet+PXT)}$ is in good agreement with the findings of previous works, where Wols et al. (2014) and Santoke and Cooper (2017) report $k_{(HO^\bullet+PXT)} = (9.6 \pm 3.6) \times 10^9 \text{ L mol}^{-1} \text{ s}^{-1}$ and $k_{(HO^\bullet+PXT)} = (8.7 \pm 0.1) \times 10^9 \text{ L mol}^{-1} \text{ s}^{-1}$, respectively. Indeed, the difference between these values is well within the variability that is usually found during the determination of second-order kinetic constants with different experimental procedures (see, for instance, Berto et al., 2018). Data fit also yielded $R_{f,HO^\bullet} = 9.6 \pm 1.5 \text{ nmol L}^{-1} \text{ s}^{-1}$ and $R_{add} = 7.6 \pm 0.6 \text{ nmol L}^{-1} \text{ s}^{-1}$. Note that R_{add} was pretty high, suggesting that the reactivity of PXT with X^\bullet would not be negligible.

3.1.3 PXT reactivity towards singlet oxygen (1O_2)

Aqueous solutions (5 mL) containing PXT (from 5 to 20 $\mu\text{mol L}^{-1}$) and the dye Rose Bengal (10 $\mu\text{mol L}^{-1}$) were irradiated under a Philips TL D 18W/16 Yellow to assess the second-order rate

constant $k_{(^1O_2+PXT)}$ of the reaction $PXT + ^1O_2$ (Vione, 2020). The excited triplet state of RB ($^3RB^*$), which is generated following light absorption by RB, is able to efficiently react with dissolved oxygen in its ground triplet state to produce 1O_2 . The majority of 1O_2 undergoes deactivation by collision with the surrounding water molecules, with a quenching rate constant $k_{q,^1O_2} = 2.5 \times 10^5 \text{ s}^{-1}$ (Wilkinson et al., 1995). The remaining fraction of 1O_2 can react with PXT (**Scheme 1**).

The rate of PXT transformation by 1O_2 is $R = k_{(^1O_2+PXT)} \times [^1O_2] \times [PXT]$, where $[^1O_2]$ is the steady-state concentration of singlet oxygen. The steady-state condition was here provided by (i) steady irradiation; (ii) partitioning of dioxygen between the irradiated solution and the headspace of the glass cell; (iii) regeneration of the RB ground-state after $^3RB^*$ quenching; (iv) continuous formation of 1O_2 upon RB irradiation, and (v) fast quenching of 1O_2 by water (**Scheme 1**). By considering the formation rate of 1O_2 by irradiated RB ($R_{f,^1O_2}$), one has $[^1O_2] = R_{f,^1O_2} (k_{q,^1O_2} + k_{(^1O_2+PXT)} \times [PXT])^{-1}$. In our case it was determined $R_{f,^1O_2} = (6.5 \pm 0.6) \times 10^{-7} \text{ mol L}^{-1} \text{ s}^{-1}$ by measuring the degradation rate of furfuryl alcohol (FFA, $100 \mu\text{mol L}^{-1}$) upon reaction with 1O_2 . The use of FFA as 1O_2 probe to measure $R_{f,^1O_2}$ has been widely adopted and described in previous works (Carena et al., 2017; Rosario-Ortiz and Canonica, 2016; Vione, 2020).

Note that the rate constants for the reaction between organic pollutants and 1O_2 in water often range between 10^6 - $10^7 \text{ L mol}^{-1} \text{ s}^{-1}$ (Arnold et al., 2017; Wilkinson et al., 1995). If this is our case as well, it should be $k_{(^1O_2+PXT)} \times [PXT] \ll k_{q,^1O_2}$ in the adopted [PXT] range (5 - $20 \mu\text{mol L}^{-1}$).

Therefore, the PXT degradation rate by 1O_2 can be linearly related to [PXT] as in **Eq. 8**:

$$R = \frac{R_{f,^1O_2} \times k_{(^1O_2+PXT)}}{k_{q,^1O_2}} \times [PXT] \quad (\text{Eq. 8})$$

A linear trend was actually found experimentally for R vs. $[PXT]$ (**Fig.S-1**), which allows for the assessment of $k_{(^1O_2+PXT)}$ from the line slope, $m = (2.06 \pm 0.17) \times 10^{-4} \text{ s}^{-1}$. By so doing, one finally gets $k_{(^1O_2+PXT)} = m \times k_{q,^1O_2} \times (R_{f,^1O_2})^{-1} = (7.9 \pm 1.4) \times 10^7 \text{ L mol}^{-1} \text{ s}^{-1}$. This value is a bit lower than, but quite comparable with that of $(1.2 \pm 0.1) \times 10^8 \text{ L mol}^{-1} \text{ s}^{-1}$ obtained by Santoke and Cooper (2017) with a competition kinetics approach.

3.1.4 Reaction of PXT with the excited triplet states of CDOM ($^3\text{CDOM}^*$)

CBBP was here used as proxy molecule for CDOM. CBBP has been widely adopted as CDOM proxy in previous works (Carena et al., 2019; Li et al., 2015; McNeill and Canonica, 2016; Wenk and Canonica, 2012). A protocol has been recently proposed based on steady irradiation experiments, to assess the reactivity of organic pollutants with the excited triplet state of CBBP ($^3\text{CBBP}^*$) (Minella et al., 2018). This protocol involves the irradiation of aqueous solutions (5 mL) containing CBBP ($\sim 70 \mu\text{mol L}^{-1}$) and different concentrations of the organic substrate S (S = PXT in our case). By studying the dependence of the S degradation rate (R) on the added S concentration ($[S]$), the value of the second-order rate constant of the reaction $S + ^3\text{CBBP}^*$ can be obtained with the following equation (Carena et al., 2019; Minella et al., 2018):

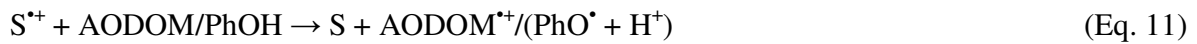
$$k_{(S+CBBP^*)} = k'_{d'} \times \left(\frac{m}{P_{0,CBBP}} - \frac{0.68 \times S_d \times k_{(^1O_2+S)}}{k_{q,^1O_2}} \right) \quad (\text{Eq. 9})$$

where $P_{a,CBBP}$ is the photon flux absorbed by CBBP, $k_d^f = 6 \times 10^5 \text{ s}^{-1}$ is the deactivation rate constant of $^3\text{CBBP}^*$ in aerated solution, 0.68 is the fraction of $^3\text{CBBP}^*$ that reacts with dissolved triplet O_2 (the remaining fraction of $^3\text{CBBP}^*$ is likely deactivated by internal conversion), $S_d = 0.46$ is the yield of $^1\text{O}_2$ upon reaction between $^3\text{CBBP}^*$ and O_2 , and $k_{q,^1\text{O}_2} = 2.5 \times 10^5 \text{ s}^{-1}$ is the $^1\text{O}_2$ quenching rate constant by collision with water molecules (**Scheme 2**). Finally, m (in s^{-1} units) is the slope of the line R vs. $[\text{S}]$.

In our case, PXT = S was irradiated under the UVA black lamp (see **Fig.S-2** for the lamp spectral photon flux density spectrum, $p^0(\lambda)$). Under these experimental conditions, the photon flux absorbed by CBBP was $P_{a,CBBP} = \int_{\lambda_1}^{\lambda_2} p^0(\lambda) \times [1 - 10^{-\epsilon_{CBBP}(\lambda) \times b \times [CBBP]}] d\lambda = (1.1 \pm 0.1) \times 10^{-8}$ Einstein $\text{L}^{-1} \text{ s}^{-1}$ ($b = 0.4 \text{ cm}$ and $[CBBP] = 70 \mu\text{mol L}^{-1}$). Note that PXT is not able to absorb radiation in the wavelength range emitted by the lamp (**Fig.1a**), thus radiation absorption by PXT was not taken into account in the calculation of $P_{a,CBBP}$. Moreover, the lack of UVA absorption by PXT also prevented its direct photolysis under UVA irradiation. **Fig.3a** shows the dependence of the PXT degradation rate on the added $[\text{PXT}]$ (from 5 to 20 $\mu\text{mol L}^{-1}$). The linear fit of the experimental data ($R^2 = 0.98$) gave $m = (8.33 \pm 0.26) \times 10^{-5} \text{ s}^{-1}$, from which $k_{(^3\text{CBBP}^* + \text{PXT})} = (4.5 \pm 0.6) \times 10^9 \text{ L mol}^{-1} \text{ s}^{-1}$ was calculated.

From the above data, the triplet-sensitized reaction of PXT looks very fast. However, several previous works have shown that the transformation reactions sensitized by $^3\text{CDOM}^*$ and $^3\text{CDOM}^*$ proxies, of some water pollutants such as anilines and sulfonamides, are inhibited by the antioxidant moieties of DOM (AODOM) (Canonica and Laubscher, 2008; Carena et al., 2019; Leresche et al., 2016; Vione et al., 2018; Wenk et al., 2011; Wenk and Canonica, 2012). In particular, $^3\text{CDOM}^*$ can partially oxidize xenobiotics through electron transfer (Davis et al.,

2018; Li et al., 2015; Wang et al., 2015), producing radicals that are then reduced back to the parent compound by AODOM (Eqs.10,11) (Wenk and Canonica, 2012). At the laboratory scale AODOM is well represented by phenol (PhOH), because it resembles anti-oxidant phenolic moieties (very common in AODOM), it is water-soluble, and it is oxidized to poorly reactive phenoxy radicals (Carena et al., 2019; Leresche et al., 2016; Vione et al., 2018; Wenk and Canonica, 2012).



If the back-reduction process induced by PhOH is operational, the actual (corrected) value of the second-order rate constant for the reaction of S with ${}^3\text{CBBP}^*$ should be $k_{(S, {}^3\text{CBBP}^*+S)}^{\text{corr}} = \psi \times k_{(S, {}^3\text{CBBP}^*+S)}$ (Vione et al., 2018), where $\psi < 1$. Because the degradation rate of S by ${}^3\text{CBBP}^*$ is $R = k_{(S, {}^3\text{CBBP}^*+S)}^{\text{corr}} \times [S] \times [{}^3\text{CBBP}^*]$, one has $R = \psi \times R^0$, where $R^0 = k_{(S, {}^3\text{CBBP}^*+PXT)} \times [S] \times [{}^3\text{CBBP}^*]$ is the transformation rate of S measured in the absence of PhOH. The correction factor ψ takes into account the back-reduction, as $\psi = (1 + [\text{PhOH}]/[\text{PhOH}]_{1/2})^{-1}$, where $[\text{PhOH}]_{1/2}$ is the phenol concentration that halves the value of R^0 (Wenk and Canonica, 2012).

$$R = \frac{R^0}{1 + \frac{[\text{PhOH}]}{[\text{PhOH}]_{1/2}}} \quad (\text{Eq. 13})$$

Fig.3b shows that the degradation rate of PXT induced by $^3\text{CBBP}^*$ decreases with increasing phenol concentration, which suggests that the back-reduction process is operational with PXT. The data fit with **Eq.13** yielded $[\text{PhOH}]_{1/2} = 1.46 \pm 0.25 \mu\text{mol L}^{-1}$.

3.1.5 Photochemical model

The photochemical fate of PXT in sunlit SW was modeled by means of the APEX software (*Aqueous Photochemistry of Environmentally-occurring Xenobiotics*) (Bodrato and Vione, 2014; Vione, 2020). The model takes into account the photoreactivity parameters of water pollutants (in the present case PXT, the photochemical parameters of which are listed in **Table 1**), sunlight irradiance, as well as the chemical composition and depth of the water body. PXT phototransformation was modeled in environmental scenarios that differed for both water depth and chemical composition (**Fig.4**). In particular, the dissolved organic carbon (DOC, which quantifies the (C)DOM content), nitrate concentration and water depth were chosen as master variables of the model. Depth was set at either 0.5 m (**Figs.4a, 4c**) or 5 m (**Figs.4b, 4d**) to represent a shallow river (or the upper layer of a lake) and a lake epilimnion, respectively. The back-reduction process was considered in the model, by converting the value of $[\text{PhOH}]_{1/2}$ ($\mu\text{mol L}^{-1}$) into a quantity that is more representative of SW ($\text{DOC}_{1/2}$, mgC L^{-1}), through the relationship $\text{DOC}_{1/2} = 0.4 \times [\text{PhOH}]_{1/2}$ (Leresche et al., 2016; Vione et al., 2018). The rate constant between PXT and $^3\text{CDOM}^*$ was thus corrected as per $k_{(^3\text{CDOM}^*+\text{S})}^{\text{corr}} = \psi \times k_{(^3\text{CBBP}^*+\text{S})}^{\text{corr}}$, with $\psi = (1 + \text{DOC}/\text{DOC}_{1/2})^{-1}$.

The pseudo-first order photodegradation rate constant of PXT (k'_{PXT}) is strongly dependent on the DOC (**Fig.4a, 4b**). This is likely due to the key roles played by $\text{CO}_3^{\cdot-}$ and HO^{\cdot} in the overall

phototransformation. The reaction of PXT with $\text{CO}_3^{\bullet-}$ and HO^\bullet prevails at low DOC values, where scavenging of the two radical species by DOM is still limited. The reverse happens at high DOC, where both $\text{CO}_3^{\bullet-}$ and HO^\bullet are very efficiently consumed by DOM.

Compared to the DOC, nitrate plays a less important role in the photodegradation kinetics of PXT (**Figs.4c, 4d**). The increase of k'_{PXT} with increasing $[\text{NO}_3^-]$ is mostly due to the enhancement of photodegradation by $\text{CO}_3^{\bullet-}$, while degradation by HO^\bullet is poorly dependent on nitrate. The most likely reason for the latter finding is that, in the presence of $5 \text{ mg}_C \text{ L}^{-1}$ DOC, CDOM would strongly out-compete nitrate in HO^\bullet generation.

The direct photolysis of PXT gets slower as the DOC increases, because of competition for irradiance between PXT and CDOM. In contrast, a variation of $[\text{NO}_3^-]$ does not affect the direct photolysis kinetics significantly, because NO_3^- is a minor radiation absorber. Interestingly, the reactions with $^3\text{CDOM}^*$ and $^1\text{O}_2$ play a secondary role in PXT photodegradation. The former process is significantly depressed by back-reduction, while PXT is poorly reactive with $^1\text{O}_2$.

Looking at the photochemical half-life times, our findings suggest that PXT is degraded fast by both direct photolysis and indirect photochemistry. Therefore, photochemical reactions are potentially important degradation pathways for PXT in SW. Lifetimes range from a few days or less in shallow waters ($d = 0.5 \text{ m}$), which are well illuminated by sunlight, up to 20-30 days in deeper waters ($d = 5 \text{ m}$) at high DOC.

3.2 Validation of the analytical methods

The HPLC-DAD method was linear in the range $10^{-6} - 10^{-4} \text{ mol L}^{-1}$ PXT ($R^2=0.9995$), with method repeatability of 1.6%. Validation parameters of the UHPLC-Qtrap method for PXT are reported in SM, **Table S-3**. As we observed that the metabolite PC partially degrades during

sample preparation, we succeeded to qualitatively determine its occurrence but its quantification was not possible.

3.3 Detection, identification and formation of TPs

Our workflow first followed the screening of the 53 candidates from our suspect list, resulting in TP-210, which has already been reported in the literature. Moreover, an additional three candidates from the predicted suspects were detected (TP-192, TP-226, TP-328).

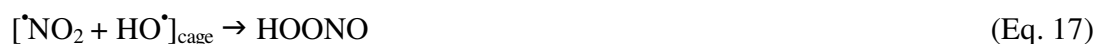
The MZmine analysis of the LC-MS data gave rise to a list of 908 features. After application of our filtering criteria (remove duplicates, retention time < 7.1 min, $100 < m/z < 500$), we were left with 453 features. In order to extract possible TP candidates, we compared blanks and control samples (withdrawn at the beginning of the experiment) with the corresponding irradiated samples using scatter plots. An example is **Fig.S-3** showing a scatter plot of a control sample, compared with a sample withdrawn after 180 minutes of irradiation, both with the addition of NaNO_3 . The ions that are placed above the chosen significance level are more abundant in the sample irradiated for 180 minutes, and thus represent potential TP candidates. This acquired list of potential TPs was also checked manually. For each of the candidates, MS/MS spectra were obtained and nine of them were identified as TPs of PXT.

All the identified TPs were detected with the positive electrospray ionization mode, while no newly formed TPs were observed in negative ionization mode. The accurate masses of the protonated molecules and MS/MS fragmentation patterns were the basis for TP identification. The level of confidence for each identified TP was assigned based on the system suggested by Schymanski et al. (2014). When no other structure fitted the experimental information, a level of

confidence 2b was assigned to the TP. If the exact location of a functional group was unknown, a level of confidence of 3 was assigned. The level of confidence 4 was assigned if we determined the elemental formula of the TP, but were unable to propose any possible structure. The isotope ratio score was obtained by MZmine “Predict molecular formula” tool. The diagnostic information for PXT and its TPs can be found in **Table 2**, and the process of assigning chemical structures to the detected TPs, including their MS/MS spectra can be found in the SM, **Chapter 2.2**.

Fig.S-16 shows the formation profiles of the TPs, which served as the basis for constructing the degradation pathway (**Fig.5**). TP-192 was formed during direct photolysis and in the reactions involving hydroxyl and carbonate radicals (**Fig.S-16: a, b, c, f**). According to the TP formation profiles in **Fig.S-16** and in line with its chemical structure, TP-192 results from the cleavage of fluorine from TP-210. A TP with $[M+H]^+$ 192 was also observed by Kwon and Armbrust (2004) during their photodegradation experiments, but the structure of the dehydrated form of TP-210 was suggested based on the MS spectra obtained with a low resolution instrument. TP-210, which was also identified as a photoproduct by Kwon and Armbrust (2004) and Šakić et al. (2013) was formed during all of our experiments, and it was one of the most abundant TPs of PXT. In contrast, TP-226 (**Fig.S-16: a, d**) and TP-238 (**Fig.S-16: c**) were formed only under certain conditions and on a smaller scale, and they likely originate from hydroxylation and formylation of TP-210. As we were not able to suggest an exact structure for TP-296, we excluded it from the predicted pathway. All the remaining TPs (TP-328, TP-350, TP-364 and TP-375) are formed from the parent molecule. While hydroxylation (TP-350, **Fig.S-16: c, d, e, f**) and oxidative defluorination (TP-328, **Fig.S-16: a, b, c, f**) are known photoreactions (Gornik et al., 2020; Hörning et al., 2012; Kosjek et al., 2013), chlorination and nitration are less common but nitration

was found to be the result of biotransformation (Kosjek et al., 2008). TP-375 was in our experiments formed specifically because of the presence of nitrates in the irradiated solution (**Fig.S-16: b, f**), which yield the nitrating agent $\cdot\text{NO}_2$ upon UV photolysis (Mack and Bolton, 1999; Vione et al., 2011):



Most reported nitrate levels in SW are below the limit of 50 mg L^{-1} , assigned in the Nitrates Directive (European Commission, 2019), while during the irradiation experiments we used a concentration that was more than ten-fold higher. Hence, the formation of TP-375 in SW is possible albeit this TP would be less abundant as compared to our experiments. The formation of TP-364 is even less probable in freshwaters. The only possible source of Cl in this experiment was the PXT reference standard itself, which is sold in the HCl salt form. The combination of UVB light, H_2O_2 and chloride probably resulted in the formation of chlorine reactive species (Vione et al., 2005) that effectively chlorinated the parent compound (**Fig.S-16: c**).

3.4 Occurrence of PXT and its TPs in actual SW

The presence of PXT, its metabolite PC and the newly identified TPs was investigated in three Slovenian SW samples. PXT concentrations were below LOQ, and no PC or TPs were detected in any sample. The first possible reason could be a lower consumption compared to the two most commonly prescribed antidepressants in Slovenia, escitalopram and sertraline, which have already been reported in Slovenian SW. Escitalopram has been reported once at a concentration of 0.42 ng L^{-1} (Klančar et al., 2018), while sertraline has been reported in three cases at concentrations of 0.24 ng L^{-1} (Klančar et al., 2018), 1.77 and 9.28 ng L^{-1} (Gornik et al., 2020). Compared to them, PXT is the fourth most commonly prescribed antidepressant in Slovenia and, based on the number of yearly prescriptions in 2019, PXT was 2.8 and 3.2 times less commonly prescribed as compared, respectively, to escitalopram and sertraline (“ZZZS - Data on drug consumption,” 2020). Other reasons may include successful removal in WW treatment plants (Cunningham et al., 2004; Duarte et al., 2019; Radjenović et al., 2007), high dilution factors, fast photodegradation, sorption to sediment or uptake into aquatic organisms.

As far as photodegradation is concerned, **Fig.6** shows the annual mean values of the photochemical half-life time of PXT in Slovenian lakes and watercourses in 2018. These values were obtained with modeling tools, based on data about the chemical composition of Slovenian water bodies that were provided by (<https://www.arso.gov.si/vode/>). A detailed description of the modeling procedure is reported in a recently published paper (Carena et al., 2021). It is seen that photochemical reactions potentially play a key role in the environmental fate of PXT, as the drug's lifetime was < 2 days in the majority ($\sim 60\%$) of the investigated water bodies, including our sampling sites. Additionally, $\text{CO}_3^{\bullet-}$ radicals and the direct photolysis should have been the main PXT phototransformation pathways, accounting for, respectively, $\sim 55\%$ and $\sim 30\%$ of the

overall PXT photodegradation (note that many Slovenian surface waters flow in karst regions, Garmo et al., 2014, providing them with pH and inorganic carbon conditions that are particularly favorable to the occurrence of $\text{CO}_3^{\bullet-}$). The remaining fraction was mainly due to reaction with HO^\bullet radicals, while the reactivity with $^3\text{CDOM}^*$ and $^1\text{O}_2$ was negligible. The fast photodegradation kinetics of PXT in Slovenian surface waters is consistent with the hypothesis that this drug does not occur in SW at significant concentration values because of effective natural attenuation.

4. Conclusions

- Direct photolysis and reaction with HO^\bullet radicals should be the main reactions that induce degradation of PXT in SW. Carbonate radicals can play an important role in PXT transformation as well, in particular at low DOC values and in the presence of high pH and inorganic carbon. PXT lifetime ranges from a few days up to a month, depending on the DOC and the water depth.
- Short lifetimes in shallow water bodies make photochemistry an important dissipation pathway for PXT in these environments.
- Reaction with $^3\text{CDOM}^*$ should be a minor degradation pathway, mostly because of the occurrence of back-reduction reactions induced by antioxidants species, which inhibit PXT degradation.
- We identified seven new TPs for PXT, and suggested benzodioxol-cleaved PXT (TP-210) as the main TP formed during photodegradation.

- The photochemical modeling of Slovenian water bodies suggests that fast photodegradation could explain why we were unable to determine either PXT, its metabolite PC or any of the identified TPs in the sampled SWs.

Slovenia is a freshwater-rich country, with high precipitation and, consequently, high dilution factors. Natural attenuation is also very likely because of very well-preserved ecosystems, with more than half of the country covered with forests and a relatively low population density. Therefore, it would be intriguing to apply the same methodology in countries that face water scarcity, high population density and a higher degree of industrialization.

Acknowledgements

The authors acknowledge financial support from the Slovenian Research Agency (research core funding No. P1-0143) and projects J1-6744 (Development of Molecularly Imprinted Polymers and their application in environmental and bio-analysis) and BI-IT-18-20-005 (Photochemical fate and treatment of pharmaceutical contaminants in drinking water). L.C. acknowledges Compagnia di San Paolo (Torino, Italy) for financially supporting his PhD fellowship. We thank Mr. Dušan Žigon (Jožef Stefan Institute) for his support in sampling campaign and HR-MS analyses, and Mr. M. Marafante (Dept. of Chemistry, University of Torino) for his help in photochemical mapping. Personnel exchange between the University of Torino and the Jožef Stefan Institute was financially supported by the bilateral cooperation agreement between Italy and Slovenia (project BI-IT-18-20-005).

References

- Arnnok, P., Singh, R.R., Burakham, R., Pérez-Fuentetaja, A., Aga, D.S., 2017. Selective Uptake and Bioaccumulation of Antidepressants in Fish from Effluent-Impacted Niagara River. *Environ. Sci. Technol.* 51, 10652–10662. <https://doi.org/10.1021/acs.est.7b02912>
- Arnold, W.A., Oueis, Y., O'Connor, M., Rinaman, J.E., Taggart, M.G., McCarthy, R.E., Foster, K.A., Latch, D.E., 2017. QSARs for phenols and phenolates: oxidation potential as a predictor of reaction rate constants with photochemically produced oxidants. *Environ. Sci. Process. Impacts* 19, 324–338. <https://doi.org/10.1039/c6em00580b>
- Berto, S., Carena, L., Chiavazza, E., Marletti, M., Fin, A., Giacomino, A., Malandrino, M., Barolo, C., Prenesti, E., Vione, D., 2018. Off-line and real-time monitoring of acetaminophen photodegradation by an electrochemical sensor. *Chemosphere* 204, 556–562. <https://doi.org/10.1016/j.chemosphere.2018.03.069>
- Bodrato, M., Vione, D., 2014. APEX (Aqueous Photochemistry of Environmentally occurring Xenobiotics): a free software tool to predict the kinetics of photochemical processes. *Environ. Sci. Process. Impacts* 16, 732–740. <https://doi.org/10.1039/c3em00541k>
- Buxton, G. V, Greenstock, C.L., Helman, P.W., Ross, A.B., 1988. Critical Review of rate constants for reactions of hydrated electrons, hydrogen atoms and hydroxyl radicals ($\cdot\text{OH}/\text{O}^{\cdot-}$) in Aqueous Solution. *J. Phys. Chem. Ref. Data* 17, 513–886. <https://doi.org/10.1063/1.555805>
- Canonica, S., 2007. Oxidation of Aquatic Organic Contaminants Induced by Excited Triplet States. *Chimia* 61, 641–644. <https://doi.org/10.2533/chimia.2007.641> *Chimia*

- Canonica, S., Laubscher, H.U., 2008. Inhibitory effect of dissolved organic matter on triplet-induced oxidation of aquatic contaminants. *Photochem. Photobiol. Sci.* 7, 547–551. <https://doi.org/10.1039/b719982a>
- Carena, L., Comis, S., Vione, D., 2021. Geographical and temporal assessment of the photochemical decontamination potential of river waters from agrochemicals: A first application to the Piedmont region (NW Italy). *Chemosphere* 263, 127921. <https://doi.org/10.1016/j.chemosphere.2020.127921>
- Carena, L., Minella, M., Barsotti, F., Brigante, M., Milan, M., Ferrero, A., Berto, S., Minero, C., Vione, D., 2017. Phototransformation of the Herbicide Propanil in Paddy Field Water. *Environ. Sci. Technol.* 51, 2695 – 2704. <https://doi.org/10.1021/acs.est.6b05053>
- Carena, L., Proto, M., Minella, M., Ghigo, G., Giovannoli, C., Brigante, M., Mailhot, G., Maurino, V., Minero, C., Vione, D., 2018. Evidence of an Important Role of Photochemistry in the Attenuation of the Secondary Contaminant 3,4-Dichloroaniline in Paddy Water. *Environ. Sci. Technol.* 52, 6334–6342. <https://doi.org/10.1021/acs.est.8b00710>
- Carena, L., Puscasu, C.G., Comis, S., Sarakha, M., Vione, D., 2019. Environmental photodegradation of emerging contaminants: A re-examination of the importance of triplet-sensitised processes, based on the use of 4-carboxybenzophenone as proxy for the chromophoric dissolved organic matter. *Chemosphere* 237, 124476. <https://doi.org/10.1016/j.chemosphere.2019.124476>
- Challis, J.K., Hanson, M.L., Friesen, K.J., Wong, C.S., 2014. A critical assessment of the photodegradation of pharmaceuticals in aquatic environments: defining our current understanding and identifying knowledge gaps. *Environ. Sci. Process. Impacts* 16, 672–696. <https://doi.org/10.1039/c3em00615h>

- Cunningham, V.L., Constable, D.J.C., Hannah, R.E., 2004. Environmental Risk Assessment of Paroxetine. *Environ. Sci. Technol.* 38, 3351–3359. <https://doi.org/10.1021/es035119x>
- Davis, C.A., McNeill, K., Janssen, E.M.L., 2018. Non-Singlet Oxygen Kinetic Solvent Isotope Effects in Aquatic Photochemistry. *Environ. Sci. Technol.* 52, 9908–9916. <https://doi.org/10.1021/acs.est.8b01512>
- Demchenko, A.P., Tomin, V.I., Chou, P., 2017. Breaking the Kasha Rule for More Efficient Photochemistry. *Chem. Rev.* 117, 13353–13381. <https://doi.org/10.1021/acs.chemrev.7b00110>
- Duarte, P., Almeida, C.M.R., Fernandes, J.P., Morais, D., Lino, M., Gomes, C.R., Carvalho, M.F., Mucha, A.P., 2019. Bioremediation of bezafibrate and paroxetine by microorganisms from estuarine sediment and activated sludge of an associated wastewater treatment plant. *Sci. Total Environ.* 655, 796–806. <https://doi.org/10.1016/j.scitotenv.2018.11.285>
- European Commission, 2019. Nitrates - Water pollution - Environment [WWW Document]. URL https://ec.europa.eu/environment/water/water-nitrates/index_en.html (accessed 4.10.20).
- Fong, P.P., 2001. Antidepressants in Aquatic Organisms: A Wide Range of Effects, in: Daughton, C.G., Jones-Lepp, T.L. (Eds.), *Pharmaceuticals and Care Products in the Environment*. American Chemical Society, Washington, DC, pp. 264–281. <https://doi.org/10.1021/bk-2001-0791.ch015>
- Fuentes, A., Pineda, M., Venkata, K., 2018. Comprehension of Top 200 Prescribed Drugs in the US as a Resource for Pharmacy Teaching, Training and Practice. *Pharmacy* 6, 43. <https://doi.org/10.3390/pharmacy6020043>

- Galbavy, E.S., Ram, K., Anastasio, C., 2010. Chemistry 2-Nitrobenzaldehyde as a chemical actinometer for solution and ice photochemistry. *J. Photochem. Photobiol. Chem.* 209, 186–192. <https://doi.org/10.1016/j.jphotochem.2009.11.013>
- Garmo, Ø.A., Skjelkvåle, B.L., de Wit, H.A., Colombo, L., Curtis, C., Fölster, J., Hoffmann, A., Hruška, J., Høgåsen, T., Jeffries, D.S., Keller, W.B., Krám, P., Majer, V., Monteith, D.T., Paterson, A.M., Rogora, M., Rzychon, D., Steingruber, S., Stoddard, J.L., Vuorenmaa, J., Worsztynowicz, A., 2014. Trends in Surface Water Chemistry in Acidified Areas in Europe and North America from 1990 to 2008. *Water. Air. Soil Pollut.* 225, 1880. <https://doi.org/10.1007/s11270-014-1880-6>
- Gornik, T., Vozic, A., Heath, E., Trontelj, J., Roskar, R., Zigon, D., Vione, D., Kosjek, T., 2020. Determination and photodegradation of sertraline residues in aqueous environment. *Environ. Pollut.* 256, 113431. <https://doi.org/10.1016/j.envpol.2019.113431>
- Henry, T.B., Kwon, J.-W., Armbrust, K.L., Black, M.C., 2004. Acute and chronic toxicity of five selective serotonin reuptake inhibitors in *Ceriodaphnia dubia*. *Environ. Toxicol. Chem.* 23, 2229–2233.
- Hörsing, M., Kosjek, T., Andersen, H.R., Heath, E., Ledin, A., 2012. Fate of citalopram during water treatment with O₃, ClO₂, UV and fenton oxidation. *Chemosphere* 89, 129–135. <https://doi.org/10.1016/j.chemosphere.2012.05.024>
- Klančar, A., Trontelj, J., Roškar, R., 2018. Development of a Multi-Residue Method for Monitoring 44 Pharmaceuticals in Slovene Surface Water by SPE-LC-MS/MS. *Water. Air. Soil Pollut.* 229, 192. <https://doi.org/10.1007/s11270-018-3845-7>
- Kosjek, T., Perko, S., Žigon, D., Heath, E., 2013. Fluorouracil in the environment: Analysis, occurrence, degradation and transformation. *J. Chromatogr. A* 1290, 62–72. <https://doi.org/10.1016/j.chroma.2013.03.046>

- Kosjek, T., Žigon, D., Kralj, B., Heath, E., 2008. The use of quadrupole-time-of-flight mass spectrometer for the elucidation of diclofenac biotransformation products in wastewater. *J. Chromatogr. A* 1215, 57–63. <https://doi.org/10.1016/j.chroma.2008.10.111>
- Kwon, J.-W., Armbrust, K.L., 2004. Hydrolysis and photolysis of paroxetine, a selective serotonin reuptake inhibitor, in aqueous solutions. *Environ. Toxicol. Chem.* 23, 1394–1399.
- Leresche, F., Von Gunten, U., Canonica, S., 2016. Probing the Photosensitizing and Inhibitory Effects of Dissolved Organic Matter by Using N,N-dimethyl-4-cyanoaniline (DMABN). *Environ. Sci. Technol.* 50, 10997–11007. <https://doi.org/10.1021/acs.est.6b02868>
- Li, Y., Wei, X., Chen, J., Xie, H., Zhang, Y. nan, 2015. Photodegradation mechanism of sulfonamides with excited triplet state dissolved organic matter: A case of sulfadiazine with 4-carboxybenzophenone as a proxy. *J. Hazard. Mater.* 290, 9–15. <https://doi.org/10.1016/j.jhazmat.2015.02.040>
- Mack, J., Bolton, J.R., 1999. Photochemistry of nitrite and nitrate in aqueous solution: a review. *J. Photochem. Photobiol. Chem.* 128, 1–13. [https://doi.org/10.1016/S1010-6030\(99\)00155-0](https://doi.org/10.1016/S1010-6030(99)00155-0)
- Matsunaga, N., Nunoya, K., Okada, M., Ogawa, M., Tamai, I., 2013. Evaluation of Hepatic Disposition of Paroxetine Using Sandwich-Cultured Rat and Human Hepatocytes. *Drug Metab. Dispos.* 41, 735–743. <https://doi.org/10.1124/dmd.112.049817>
- McDermott, S., 2018. HSE prescriptions for antidepressants and anxiety medications up by two thirds since 2009 [WWW Document]. TheJournal.ie. URL <https://www.thejournal.ie/ireland-antidepressant-anxiety-medicine-prescriptions-4157452-Aug2018/> (accessed 3.26.20).

- McNeill, K., Canonica, S., 2016. Triplet state dissolved organic matter in aquatic photochemistry: reaction mechanisms, substrate scope, and photophysical properties. *Environ. Sci. Process. Impacts* 18, 1381–1399. <https://doi.org/10.1039/C6EM00408C>
- Minella, M., Rapa, L., Carena, L., Pazzi, M., Maurino, V., Minero, C., Brigante, M., Vione, D., 2018. An experimental methodology to measure the reaction rate constants of processes sensitised by the triplet state of 4-carboxybenzophenone as a proxy of the triplet states of chromophoric dissolved organic matter, under steady-state irradiation conditions. *Environ. Sci. Process. Impacts* 20, 1007–1019. <https://doi.org/10.1039/c8em00155c>
- Mole, R.A., Brooks, B.W., 2019. Global scanning of selective serotonin reuptake inhibitors: occurrence, wastewater treatment and hazards in aquatic systems. *Environ. Pollut.* 250, 1019–1031. <https://doi.org/10.1016/j.envpol.2019.04.118>
- Myers, O.D., Sumner, S.J., Li, S., Barnes, S., Du, X., 2017. One Step Forward for Reducing False Positive and False Negative Compound Identifications from Mass Spectrometry Metabolomics Data: New Algorithms for Constructing Extracted Ion Chromatograms and Detecting Chromatographic Peaks. *Anal. Chem.* 89, 8696–8703. <https://doi.org/10.1021/acs.analchem.7b00947>
- QGIS, 2020. QGIS Geographic Information System. Open Source Geospatial Foundation Project.
- Radjenovic, J., Petrovic, M., Barceló, D., 2007. Analysis of pharmaceuticals in wastewater and removal using a membrane bioreactor. *Anal. Bioanal. Chem.* 387, 1365–1377. <https://doi.org/10.1007/s00216-006-0883-6>
- Radjenović, J., Petrović, M., Barceló, D., Petrović, M., 2007. Advanced mass spectrometric methods applied to the study of fate and removal of pharmaceuticals in wastewater treatment. *TrAC Trends Anal. Chem.* 26, 1132–1144. <https://doi.org/10.1016/j.trac.2007.10.002>

- Rosario-Ortiz, F.L., Canonica, S., 2016. Probe Compounds to Assess the Photochemical Activity of Dissolved Organic Matter. *Environ. Sci. Technol.* 50, 12532–12547. <https://doi.org/10.1021/acs.est.6b02776>
- Šakić, D., Achraimer, F., Vrček, V., Zipse, H., 2013. The chemical fate of paroxetine metabolites. Dehydration of radicals derived from 4-(4-fluorophenyl)-3-(hydroxymethyl)piperidine. *Org. Biomol. Chem.* 11, 4232. <https://doi.org/10.1039/c3ob40219c>
- Santoke, H., Cooper, W.J., 2017. Environmental photochemical fate of selected pharmaceutical compounds in natural and reconstituted Suwannee River water: Role of reactive species in indirect photolysis. *Sci. Total Environ.* 580, 626–631. <https://doi.org/10.1016/j.scitotenv.2016.12.008>
- Schultz, M.M., Furlong, E.T., Kolpin, D.W., Werner, S.L., Schoenfuss, H.L., Barber, L.B., Blazer, V.S., Norris, D.O., Vajda, A.M., 2010. Antidepressant pharmaceuticals in two US effluent-impacted streams: occurrence and fate in water and sediment, and selective uptake in fish neural tissue. *Environ. Sci. Technol.* 44, 1918–1925.
- Schymanski, E.L., Jeon, J., Gulde, R., Fenner, K., Ruff, M., Singer, H.P., Hollender, J., 2014. Identifying Small Molecules via High Resolution Mass Spectrometry: Communicating Confidence. *Environ. Sci. Technol.* 48, 2097–2098. <https://doi.org/10.1021/es5002105>
- Silva, L.J.G., Pereira, A.M.P.T., Meisel, L.M., Lino, C.M., Pena, A., 2015. Reviewing the serotonin reuptake inhibitors (SSRIs) footprint in the aquatic biota: Uptake, bioaccumulation and ecotoxicology. *Environ. Pollut.* 197, 127–143. <https://doi.org/10.1016/j.envpol.2014.12.002>
- Turro, N.J., Ramamurthy, V., Cherry, W., Farneth, W., 1978. The Effect of Wavelength on Organic Photoreactions in Solution. Reactions from Upper Excited States. *Chem. Rev.* 78, 125–145. <https://doi.org/10.1021/cr60312a003>

- US Environmental Protection Agency, 2016. Final Report, The Environmental Occurrence, Fate, and Ecotoxicity of Selective Serotonin Reuptake Inhibitors (SSRIs) in Aquatic Environments, Research Project Database, NCER | ORD | US EPA [WWW Document]. URL https://cfpub.epa.gov/ncer_abstracts/index.cfm/fuseaction/display.highlight/abstract/1755/report/F (accessed 3.7.16).
- Vasskog, T., Anderssen, T., Pedersen-Bjergaard, S., Kallenborn, R., Jensen, E., 2008. Occurrence of selective serotonin reuptake inhibitors in sewage and receiving waters at Spitsbergen and in Norway. *J. Chromatogr. A* 1185, 194–205. <https://doi.org/10.1016/j.chroma.2008.01.063>
- Vasskog, T., Berger, U., Samuelsen, P.-J., Kallenborn, R., Jensen, E., 2006. Selective serotonin reuptake inhibitors in sewage influents and effluents from Tromsø, Norway. *J. Chromatogr. A* 1115, 187–195. <https://doi.org/10.1016/j.chroma.2006.02.091>
- Vay, M., Majewsky, M., Mikus, G., 2018. Isotopically labelled paroxetine standard allows for definite structure elucidation of the paroxetine tandem mass spectrum. *Rapid Commun. Mass Spectrom.* 32, 1311–1312. <https://doi.org/10.1002/rcm.8178>
- Vione, D., 2020. A Critical View of the Application of the APEX Software (Aqueous Photochemistry of Environmentally-Occurring Xenobiotics) to Predict Photoreaction Kinetics in Surface Freshwaters. *Molecules* 25, 9. <https://doi.org/10.3390/molecules25010009>
- Vione, D., Maurino, V., Minero, C., Calza, P., Pelizzetti, E., 2005. Phenol chlorination and photochlorination in the presence of chloride ions in homogeneous aqueous solution. *Environ. Sci. Technol.* 39, 5066-5075. <https://doi.org/10.1021/es0480567>

- Vione, D., Sur, B., Dutta, B. K., Maurino, V., Minero, C., 2011. On the effect of 2-propanol on phenol photonitration upon nitrate photolysis. *J. Photochem. Photobiol. A: Chem.* 224, 68-70. <https://doi.org/10.1016/j.jphotochem.2011.09.008>
- Vione, D., Minella, M., Maurino, V., Minero, C., 2014. Indirect photochemistry in sunlit surface waters: Photoinduced production of reactive transient species. *Chemistry Eur. J.* 20, 10590-10606.
- Vione, D., Fabbri, D., Minella, M., Canonica, S., 2018. Effects of the antioxidant moieties of dissolved organic matter on triplet-sensitized phototransformation processes: Implications for the photochemical modeling of sulfadiazine. *Water Res.* 128, 38–48. <https://doi.org/10.1016/j.watres.2017.10.020>
- von Sonntag, C., Schuchmann, H.-P., 1991. The Elucidation of Peroxyl Radical Reactions in Aqueous Solution with the Help of Radiation-Chemical Methods. *Angew Chem Int Ed Engl* 30, 1229–1253. <https://doi.org/doi:10.1002/anie.199112291>
- Wang, S., Song, X., Hao, C., Gao, Z., Chen, J., Qiu, J., 2015. Elucidating triplet-sensitized photolysis mechanisms of sulfadiazine and metal ions effects by quantum chemical calculations. *Chemosphere* 122, 62–69.
- Wenk, J., Canonica, S., 2012. Phenolic antioxidants inhibit the triplet-induced transformation of anilines and sulfonamide antibiotics in aqueous solution. *Environ. Sci. Technol.* 46, 5455–5462. <https://doi.org/10.1021/es300485u>
- Wenk, J., Von Gunten, U., Canonica, S., 2011. Effect of Dissolved Organic Matter on the Transformation of Contaminants Induced by Excited Triplet States and the Hydroxyl Radical. *Environ. Sci. Technol.* 45, 1334–1340. <https://doi.org/10.1021/es202028w>
- Wilkinson, F., Helman, W.P., Ross, A.B., 1995. Rate Constants for the Decay and Reactions of the Lowest Electronically Excited Singlet State of Molecular Oxygen in Solution. *An*

- Expanded and Revised Compilation. *J. Phys. Chem. Ref. Data* 24, 663.
<https://doi.org/10.1063/1.555965>
- Willett, K.L., Hites, R.A., 2000. Chemical Actinometry : Using o-Nitrobenzaldehyde to Measure Light Intensity in Photochemical Experiments. *J. Chem. Educ.* 77, 900–902.
<https://doi.org/10.1021/ed077p900>
- Wojnárovits, L., Tóth, T., Takács, E., 2020. Rate constants of carbonate radical anion reactions with molecules of environmental interest in aqueous solution: A review. *Sci. Total Environ.* 717, 137219. <https://doi.org/10.1016/j.scitotenv.2020.137219>
- Wols, B.A., Harmsen, D.J.H., Beerendonk, E.F., Hofman-caris, C.H.M., 2014. Predicting pharmaceutical degradation by UV (LP)/ H₂O₂ processes: A kinetic model. *Chem. Eng. J.* 255, 334–343. <https://doi.org/10.1016/j.cej.2014.05.088>
- Wu, C., Witter, J.D., Spongberg, A.L., Czajkowski, K.P., 2009. Occurrence of selected pharmaceuticals in an agricultural landscape, western Lake Erie basin. *Water Res.* 43, 3407–3416. <https://doi.org/10.1016/j.watres.2009.05.014>
- Zhao, S.X., Dalvie, D.K., Kelly, J.M., Soglia, J.R., Frederick, K.S., Smith, E.B., Obach, R.S., Kalgutkar, A.S., 2007. NADPH-Dependent Covalent Binding of [³H]Paroxetine to Human Liver Microsomes and S-9 Fractions: Identification of an Electrophilic Quinone Metabolite of Paroxetine. *Chem. Res. Toxicol.* 20, 1649–1657.
<https://doi.org/10.1021/tx700132x>
- ZZZS - Data on drug consumption [WWW Document], 2020. URL https://partner.zzs.si/wps/portal/portali/aizv/zdravila_in_zivila_za_posebne_zdravstvene_namene/podatki_o_porabi_zdravil!/ut/p/z1/04_Sj9CPykssy0xPLMnMz0vMAfj08ziTQxdPd2N_Q08LSyCDQ0cjZzMzXz8XQ0sTAz0C7IdFQGdnpEx/ (accessed 6.10.20).